Check dam impact on sediment loads: example of the Guerbe River in the Swiss Alps - a catchment scale experiment

Ariel Henrique do Prado[1], David Mair[1], Philippos Garefalakis[1], Chantal Schmidt[1], Alexander C. Whittaker[2], Sebastien Castelltort[3] and Fritz Schlunegger[1]

[1] University of Bern, Institute of Geological Sciences, Bern, Switzerland

[2] Imperial College, Department of Earth Science and Engineering, London, United Kingdom

[3] University of Geneva, Department of Earth Sciences, Geneva, Switzerland

Correspondence to: Ariel do Prado (ariel.doprado@geo.unibe.ch)

Abstract

The construction of check dams is a common practice around the world where the aim is to reduce the damage by flooding events through mountain streams. However, quantifying the effectiveness of such engineering structures has remained very challenging and requires well-selected case studies, since the outcome of such an evaluation depends on site specific geometric, geologic, and climatic conditions. Conventionally, the check dams' effectiveness has been estimated using information about how the bedload sediment flux in the stream changes after the check dams are constructed. A permanent lowering of the bedload flux not only points to a success in reducing the probability of sediment transport occurrence but also implies that the sediment input through the system is likely to decrease. Here, we applied a method for data acquisition and two different equations (Meyer-Peter Müller and Recking approach) to estimate and compare the sediment transport in a mountain stream in Switzerland under engineered and non-engineered conditions. Whereas the first equation is derived from a classical approach that is based on flume experiment data with a slope less than 0.02 m/m, the second equation (Recking) has been deviated based on a bedload field data set comprising active mountain streams under steeper conditions. We selected the Guerbe River situated in the Swiss Alps as a case study, which has been engineered since the end of the 19th century. This has resulted in more than 110 check dams along a c. 5 km reach where sediment has continuously been supplied from adjacent hillslopes, primarily by landsliding. We measured the riverbed grain size, topographic gradients, and river widths within selected segments along this reach. Additionally, a gauging station downstream of the reach engineered with check dams yielded information to calibrate the hydroclimatic situation for the study reach, thus offering ideal conditions for our catchment-scale experiment. Using the acquired data and the dataset about historical runoff covering the time interval between 2009 and 2021 and considering the current engineered conditions, we estimated a mean annual volume of transported bedload which ranges from 900 to 6'000 m^3 yr^{-1}. We then envisaged possible channel geometries before the check dams were constructed. We inferred (1) higher energy gradients which we averaged over the length of several check dams and which we considered as a proxy for the steeper river slope under natural conditions; (2) channel widths that are smaller than those measured today, thereby anticipating that the channel was more confined in the past; and (3) larger grain size percentiles, which we consider to be

similar to the values measured from preserved landslides in the region. Using such potential non-engineered scenarios as constraints, the two equations both point towards a larger sediment flux compared to the engineered state, although the results of these equations differed significantly in magnitude. Whereas the Recking approach returned estimates where the bedload sediment flux is c. 10 times larger in comparison with the current situation, the use of the Meyer-Peter Müller equation predicts an increase of c. 100 times in bedload fluxes for a state without check dams. These results suggest that the check dams in the Guerbe (Gürbe) River are highly efficient not only in regulating sediment transport by decreasing the probability of high sediment flux occurrence during torrential conditions, but also in stabilizing the channel bed by avoiding incision. The most likely consequence is a stabilization of the terrain around such structures by reducing the activation of landslides.

1. Introduction

Engineering structures known as check dams have been constructed in many mountainous streams around the world with the intention to mitigate hazards caused by the transfer of large volumes of sediment in relation to flooding, landsliding and debris flows (Piton et al., 2017; Lucas-Borja et al., 2021). Check dams are transversal structures built across the channel bed and made of wood, rock or concrete. They create space that can initially store sediment derived from farther upstream. Subsequently, this space is filled with material, which diminishes its capacity to store additional sedimentary material. However, even in their filled stages, the check dams seem to remain operational for two reasons. First, they prevent the stream from further incising into substratum, which in turn contributes to the stabilization of landslides and the preservation of soils on the bordering hillslopes; second, they reduce the stream's capacity to evacuate the supplied sedimentary material due to a reduction of the channel's friction slope; and third, they contribute to the regulation of sediment transport by buffering the release of sediment into more frequent and lower discharges of material (Castillo et al., 2014; Piton et al., 2017). Although it is generally appreciated that the construction of check dams is beneficial for reducing risks, it has been a recurring challenge for engineers and the different stakeholders to take decisions about whether or not to install such infrastructure because of the high maintenance costs (e.g., Jackle, 2013; Ramirez, 2022) and also because of bio-environmental concerns (Bombino et al., 2014). Furthermore, in most of these streams, the construction of check dams started before a survey on sediment flux was conducted, with the consequence that information about the pre-engineered conditions on sediment discharge is not available (Piton et al., 2017). Hence, it remains difficult to quantify the efficiency of such infrastructure, and society is left with limited information for taking decisions on whether or not to build new check dams and/or to maintain older ones. Under these circumstances, an indirect method of estimating the contribution of check dams to reduce risks is needed for stakeholders when they have to take evidence-based decisions on how to manage such infrastructure. In the past decade, Castillo et al. (2014) developed a model to estimate the efficiency of check dams. They focussed on exploring how the variations of the friction slope angles, which varied through changing the spacing between the dams, impacted the flow regime. However, since the friction slope is not the only variable that controls the transport of sediment (e.g., Meyer-Peter and Müller, 1948; Wong and Parker, 2006 ; Piton and Recking, 2016; Recking et al., 2016), data on slope changes

alone is not sufficient to fully appreciate and predict possible reductions of risks when check dams are set in place. As an alternative approach, estimates of the sediment volumes transported on the riverbed could be used to predict the efficiency of check dams once the space behind them has been filled (Kaitna et al., 2011; Piton et al., 2017; Keiler and Fuchs, 2018). Therefore, available bedload equations that were calibrated on data acquired in active streams and flume experiments are potential tools for such an evaluation, and their application depends on variables that can be measured in the field (e.g., slope, width, and grain size distributions).

To do so, we studied the Guerbe River, which is a torrent situated on the northern margin of the Swiss Alps (Fig. 1). There, the c. 5 km-long headwater reach has experienced a >100-year-long history of check dam construction and maintenance. The first ones were installed during the 19th century and mainly consisted of structures made of wood and stone (Salvisberg, 2017). Subsequently, they were replaced by reinforced concrete dams in the 20th century, forming steps that are up to 10 m high (e.g., Fig. 1b). However, during several events along their history, the check dams failed and released a large amount of material to downstream of the channel generating a large loss to the local society (Salvisberg, 2017). After the last failure event, which occurred in January 2018 with the displacement of the c. 4.5 x 10^6 m^3-large Meierisli landslide that damaged >10 of these check dams (Andres and Badoux, 2019), the local community has been confronted with taking a decision on how to manage this situation in the future without a-priori, physics-based information on the efficiency of this infrastructure. Therefore, this paper aims to offer such a quantitative evaluation. Here, we estimate the efficiency regarding the transport of bedload material for a staircase of check dams using the Guerbe River as a natural laboratory. We collect high-resolution data on the channel's metrics (slope, width) and the grain size distribution in the field, and we combine this data with information about the hydroclimatic properties of the Guerbe River basin. The scope is to estimate the modern bedload sediment flux for the current engineered state. These results are then compared with the outcome of model runs where pre-engineered conditions regarding channel metrics (slope, width) and grain size distributions are considered.

2. Local setting

The studied reach of the Guerbe River (Fig. 1a), which is situated at the northern border of the Swiss Alps, can be segmented into four parts: (1) The headwater reach, which is the uppermost segment covering an area of c. 5 km^2, is characterized by a dendritic network made up of first to third-order channels. The stream originates in the Gantrisch area at an altitude of c. 1800 m a.s.l. where the bedrock is made up of steeply dipping limestones, dolostones and marls that are part of the Penninic Klippen belt (Jäckle, 2013). Towards the lower part of the headwater reach, the Mesozoic units are covered by several meters-thick glacial till. This headwater reach transitions into a steep segment at an elevation of c. 1200 m a.s.l. where the longitudinal stream profile of the Guerbe River shows a knickpoint (next to site 1 in Fig. 1 and circle in Fig. 2). The occurrence of such a knickpoint in the stream profile is also seen in the morphology of the bordering hillslopes where slope angles are c. 20-25° steep. These hillslopes constitute an important sediment source of the Guerbe River. Uphill, these hillslopes mark a sharp transition towards a flatter landscape that was originally formed by glaciers, thereby defining also a knickzone on the hillslopes (Fig. 2). The second segment occurs downstream of this knickzone area, where the Guerbe River has been fully engineered by > 60 check dams. There, the bedrock comprises a

suite of Late Cretaceous to Paleocene Gurnigel Flysch and the Early Oligocene Lower Marine Molasse (L.M.M.) units, both of which are alternations of shales and sandstones. They are dissected by multiple landslides along the entire c. 2 km-long second segment of the Guerbe River (Red segment in Fig. 1). These landslides either originate >1 km upstream of the Guerbe channel and are deep-seated with a decollement horizon up to 20 m below the surface (Thuner Tagblatt, 25th of Mai 2018), or they border the Guerbe trunk stream as a few shallow-seated and < 100 m-long features (decollement < 2 m deep) as own observations have shown. Along this second reach, the Guerbe River shows a "colluvial" stream pattern as defined by Piton and Recking (2017). The third segment comprises the reach along which the river then transitions on a c. 4 km^2-large alluvial fan where the apex is located at an elevation of c. 800 m a.s.l (white segment in Fig. 1). The stream remains channelized and with presence of check dams on the entire fan. In the final segment, the stream enters the floodplain area, where it flows in a confined channel until its confluence with the Aare River c. 20 km farther downstream.

The climate in the region is typical for a pre-alpine setting with a mean annual precipitation rate that ranges between 2000 mm yr^{-1} in the mountains and 1100 mm yr^{-1} at lower elevations (Ramirez et al., 2022). Accordingly, the mean annual water discharge is c. 1.3 m^3 s^{-1} as recorded by the Burgistein gauging station c. 4 km downstream of the source area, and the maximum discharge during the past 22 years has been 84 m^3 s^{-1}, measured on the 29th of July in 1990 (Ramirez et. al, 2022). Peak water flux occurs either during convective thunderstorms in summer or during periods of extended precipitation in late spring and fall. In addition, a denudation rate of c. 260 mm/kyr on our surveyed catchment was estimated from ^{10}Be concentrations obtained from riverine quartz minerals in the Guerbe River (Delunel et al., 2020).

3. Methods and datasets

To assess the impact of check dams on bedload fluxes, we compare the results of bedload equations, which are either based on the results of flume experiments (e.g. Meyer-Peter and Müller, 1948; Einstein, 1950; Bagnold, 1980; Wong and Parker, 2006; Parker, 2008; Recking et al., 2012) and/or field-based surveys (e.g. Karim and Kennedy, 1990; Recking, 2013; Recking et al., 2016). These equations were calibrated and validated under specific conditions of grain sizes, slopes, and channel dimensions. They are not expected to provide precise predictions for bedload fluxes under extrapolated boundary conditions. Indeed, all equations present large uncertainties when used to estimate bedload flux for single events under the same boundary conditions, showing uncertainties of ± 1 order of magnitude in the best scenarios (Rickenmann, 2001; Recking et al., 2012). Despite this limitation, these equations were adjusted to represent the average bedload flux under natural conditions. Therefore, they remain valuable tools when used in a relative manner for estimating changes in sediment transport capacity between engineered and non-engineered conditions in the Guerbe River.

Among the various bedload equations that have been published in the scientific literature, we chose to consider the Meyer-Peter and Müller (1948) and Recking (2013) equations, as they are representative of the two families of equations derived from flume and field data, respectively. However, their application requires that some geometric requirements regarding the spacing between check dams and the resulting flow conditions are

fulfilled. These are described in section 3.1. Following is the introduction of the selected bedload equations used in this work (section 3.2), and the description of the methods to acquire the data to estimate the sediment fluxes. Finally, we describe the considerations for the non-engineered conditions in our estimations (section 3.4).

3.1. Flow specificities related to check dams

One important functioning of the filled check dams is to reduce the kinetic energy of a mountain stream, which in turn is expected to reduce the sediment load (Castillo et al., 2014). In the reach downstream of a check dam, the largest energy dissipation occurs when the water that falls from the check dam spillway impacts the ground. The water enters a high-turbulent flow stage, thereby creating a scour and thus a pool just at the foot of the check dam (e.g. Fig. 3). A second contribution to the energy dissipation derives from the basal friction exerted by the arrangement of clasts along the river bed as the water leaves the pool (Piton and Recking, 2016). The flow is then more uniform, and local turbulences occur less frequently. The spacing between two adjacent check dams can affect this pattern when the distance is shorter than $30 h_c$ (where h_c is the critical depth for which the Froude number is equal to 1; Piton and Recking, 2016), which is not the case for the Guerbe River since the spacing between the check dams is > 20 m and the maximum critical flow depth is 0.43 m at the apex of the alluvial fan (calculation done by using the measurements presented in the results section). This assumption is key for the application of the bedload equations presented in section 3.2 since it requires the occurrence of a near-uniform flow.

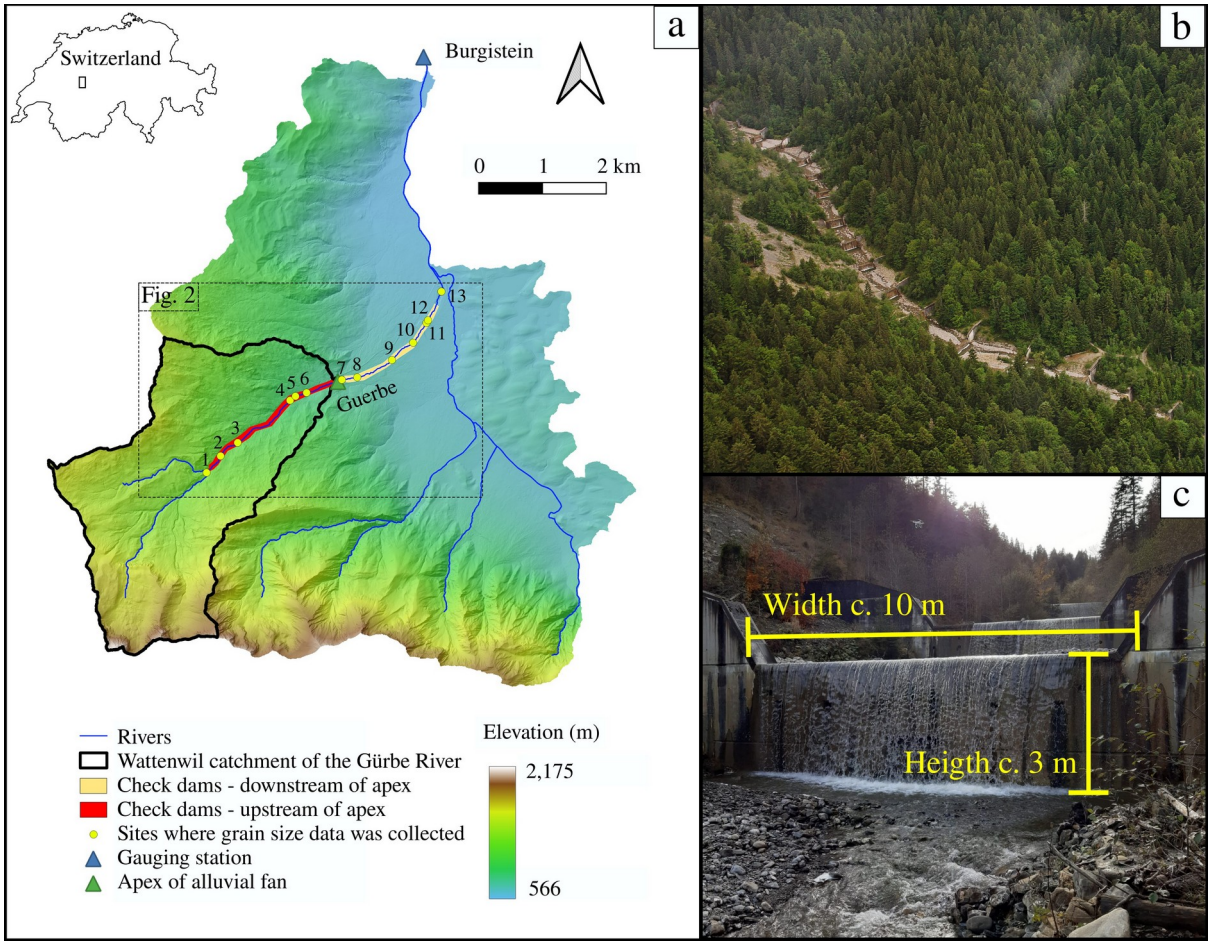

Figure 1. (a) DEM of the Guerbe catchment upstream of the Burgistein gauging station, and sub-catchment where sediment has been produced and supplied to the trunk channel (Wattenwil catchment of the Guerbe River). The dashed rectangle limits the area shown in Fig. 2. (b) Aerial picture in the Guerbe River with the staircase check dams. Additionally, the picture shows a steep non-vegetated area where recent hillslope instabilities have prevented a dense vegetation cover to establish (c) Example of check dams with heights of c. 3 m.

3.2. Bedload discharge in mountain streams

Flume-based equations to estimate the volumes of bedload transported by streams have generally been developed for rivers with slopes < 0.02 m m^{-1} (or 1.2 degrees) and riverbed material composed of grains with sizes that range from coarse sand to coarse gravel (e.g. Meyer-Peter and Müller, 1948; Einstein, 1950; Bagnold, 1980; Wong and Parker, 2006; Parker, 2008; Recking et al., 2012). In mountain streams, where slopes are usually steep (> 0.02 m m^{-1}) and where the size of the transported material ranges from gravel to boulders, these equations tends to overestimate the bedload fluxes (Lamb et al., 2008). We selected the MP.M. equation due its simplicity, suitability for the gravel grain size domain, and due its capability of being adapted for slopes steeper than 0.02 m m^{-1}. For such steep reaches, we considered a correction for the critical Shields shear stress (Lamb et al., 2008; Recking et al., 2012; Shvidchenko et al., 2001). Additionally, we employed the Wong and Parker

(2006) formulation, which is an updated and corrected version of the Meyer-Peter and Müller (1948) formula. The selected field-based formulation proposed by Recking (2013), reformulated by Recking et al. (2016), considers different channel morphologies and was evaluated and validated for steep and coarse-grained mountain streams similar to the Guerbe River (Piton and Recking, 2017). Therefore, this equation may be suited for estimating the bedload flux in our study case. Furthermore, it is important to note that in mountain streams, the amount of transported material is influenced by its availability. In this study, we clarify that bedload flux calculations are interpreted as the capacity of the torrent to transport material under specified boundary conditions.

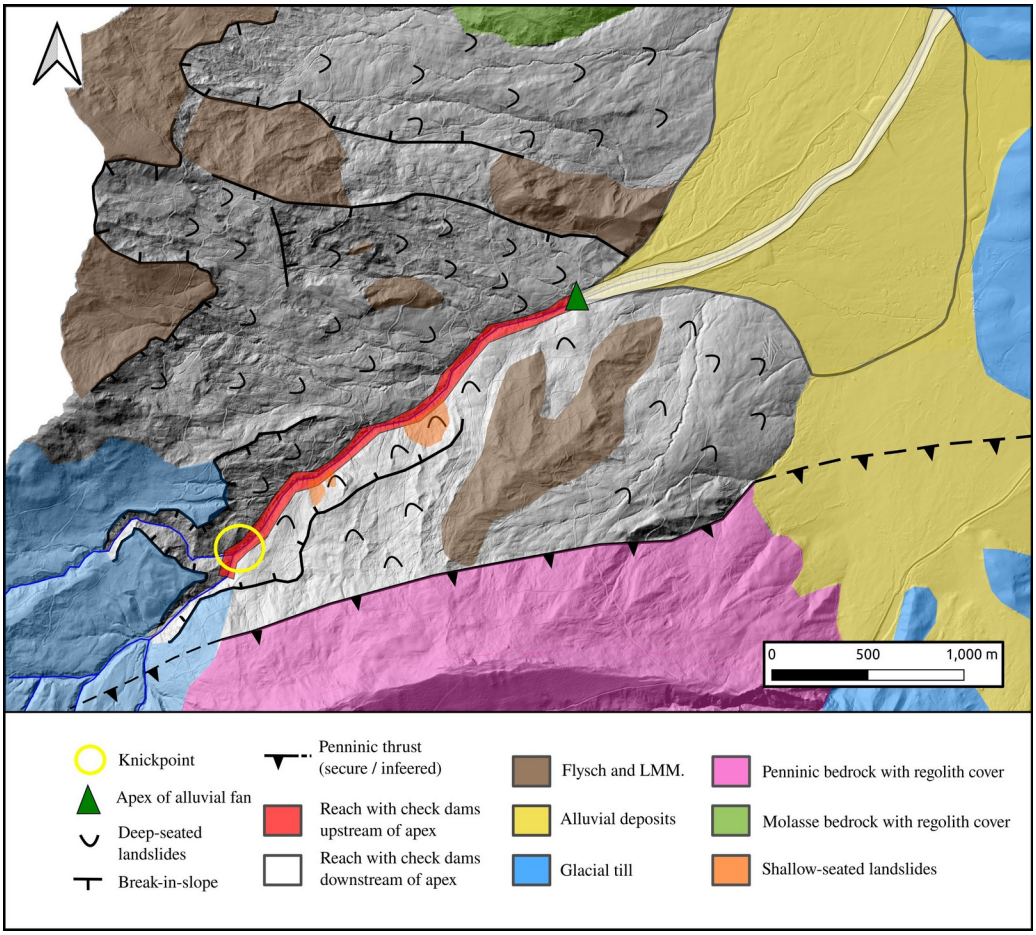

Figure 2. Map of the landslides and incised areas of the Guerbe River together with the bedrock geology underlying the catchment. The knickpoint is located inside the yellow circle. See Fig. 1 for the position of this map. Here the LMM denotes the Lower Marine Molasse.

For both the MP.M. and Recking approaches we calculated the total bedload sediment flux (Q_s) by computing the dimensionless sediment bedload flux, with the Einstein parameter (Φ) (Einstein, 1950):

$$Q_s = \phi \cdot W \cdot \sqrt{g \cdot (\rho_s / \rho_w - 1) \cdot D_{50}^3} \quad (1)$$

Where Q_s is the total bedload sediment flux (m^3/s), W is the active river width (m), g is the gravity acceleration (m^2/s), ρ_s and ρ_w (kg/m^3) are the densities of sediment and water, respectively, and D_{50} (m) is the 50th percentile of the riverbed surface grain sizes (b-axis) and here represents the characteristic diameter of the transported material. In the following, we present the formulation to calculate Φ using the MP.M. and Recking approaches.

3.2.1 Dimensionless sediment bedload flux (Φ) based on MP.M. approach

For an alluvial stream where water flow is considered uniform, the Einstein parameter (Φ) can be calculated by the formulation proposed by Wong and Parker (2006):

$$\phi = A \cdot \left(\tau^* - \tau_c^* \right)^{1.5} \quad (2)$$

Where A is a non-dimensional constant, which was set to 3.97 by Wong and Parker (2006) based on a reanalysis of the dataset obtained by Meyer-Peter and Müller (1948) through flume experiments. In this equation, the difference between the dimensionless shear stress (τ^*) and the Shields (1936) parameter (τ_c^*) is key for estimating how much sediment a stream can entrain from the riverbed if $\tau^* \geq \tau_c^*$. For a non-uniform mixture of grains on a riverbed, the choice of the D_{50} in Eq. 1 is justified for near-equal mobility conditions when grains larger and smaller than the D_{50} are mobilised at nearly the same rate and for the same shear stress (Julien, 2010). While Wong and Parker (2006) considered a constant value $\tau_c^* = 0.0495$ for the Shields number, Lamb et al. (2008) proposed to employ a slope-dependent correction, mainly because the consideration of a constant Shields number will overpredict the bedload discharge in Eq. 1 for steep gradients (> 0.02), which is the case for the Guerbe River. Therefore, we considered the Shields parameter (τ_c^*) to be dependent on the channel bed gradient S (in meter per meter) following the results of field and laboratory experiments (Lamb et al., 2008):

$$\tau_c^* = 0.15 \cdot S^{0.25} \quad (3)$$

The dimensionless shear stress (τ^*) is defined following Shields (1936):

$$\tau^* = \frac{\tau}{g \cdot (\rho_s - \rho_w) \cdot D_{50}} \quad (4)$$

The shear stress (τ) in a river bed is controlled by the channel depth d (in meters) for streams where the river width is $W > 20\ d$:

$$\tau = \rho_w \cdot g \cdot d \cdot S \quad (5)$$

Here we considered that the channel has a rectangular configuration. In the case of a uniform flow, the friction slope can be considered as being identical to the alluvial riverbed slope ($S = S_{bed}$). The water depth is calculated from the relationship between the unit water discharge ($q = Q \cdot W^{-1}$; $m^2\ s^{-1}$) and the mean water velocity along the river depth v (expressed in meters per second):

$$d = \frac{q}{v} \tag{6}$$

Ferguson (2007) proposed that in a stream, the mean water velocity (v) of a water column can be calculated separately for shallow- and deep-water conditions thereby using the Manning Strickler friction law and a roughness layer (MS/RL) term:

$$v_d = \frac{{a_1}^{0.6} \cdot g^{0.3} \cdot S^{0.3} \cdot q^{0.4}}{D_{84}^{0.1}} \quad \text{(deep flows)} \tag{7.1},$$

and

$$v_s = \frac{{a_2}^{0.4} \cdot g^{0.2} \cdot S^{0.2} \cdot q^{0.6}}{D_{84}^{0.4}} \quad \text{(shallow flows)} \tag{7.2}.$$

Here a_1 and a_2 are empirically obtained values and set to 5.5 and 2.5 (Ferguson, 2007), and the D_{84} is the 84th percentile of the riverbed grain sizes (b-axis). The water column is considered as "shallow" if $d / D_{84} < 4$, else it is considered as deep. This formula has the advantage that it can be applied to rivers with a large range of slopes, including those encountered in mountainous streams where the slopes are steep (Zimmermann, 2010).

3.2.2 Dimensionless sediment bedload flux (Φ) based on the empirically calibrated Recking approach

A further method for calculating the reach-average bedload flux for gravelly rivers was proposed by Recking (2013). The related equations were empirically adjusted using a large dataset collected in the field, and they were validated by blind tests, which were conducted for 15 river reaches. According to this author, the Einstein parameter (Φ) can be calculated through:

$$\phi = \frac{14\,{\tau^*}^{2.5}}{1+\left(\frac{{\tau_m}^*}{\tau^*}\right)^4} \tag{8}$$

Where τ^* is the dimensionless shear stress defined in Eq. 4. The parameter ${\tau_m}^*$ accounts for the transition from the situation where only a fraction of the channel bed material is transported (partial transport) to the condition where all sedimentary material is in transport (full mobility). The original formula presented in 2013 was subsequently updated by Recking et al. (2016) to account for streams with flatbeds and step-pool patterns:

$${\tau_m}^* = 1.5 \cdot S^{0.75} \tag{9}$$

In Eq. 8 the dimensionless shear stress τ^* is defined by Eq. 4, which is dependent on the flow depth (d) to estimate the shear stress (Eq. 5). In the following, we calculated the flow depth using the equation derived by

Recking et al. (2016), which itself bases on the flow resistance formula proposed by Rickenmann and Recking (2011):

$$d = 0.015 \cdot D_{84} \frac{q^{*2p}}{p^{2.5}} \quad (10)$$

where $q^* = q/\sqrt{g \cdot S \cdot D_{84}^3}$ and $p = 0.24$ if $q^* < 100$, else $p = 0.31$. Therefore, we re-calculated the dimensionless shear stress in the following way:

$$\tau^* = \frac{0.015 \cdot q^{2p} \cdot D_{84}^{1-3p} \cdot S^{1-p}}{p^{2.5} \cdot g^p \cdot (\rho_s/\rho_w - 1) \cdot D_{50}} \quad (11)$$

Piton and Recking (2017) used the Recking et al. (2016) formula to calculate the bedload flux considering different states of armouring on the channel bed and various sources of sediment. They compared the suitability of the equation to predict the bedload flux by using two different values as the characteristic diameter of the transported material: the 84th grain size percentile of the bedload material in transport labelled as $D_{84,TraBL}$ and the 84th percentile of the riverbed surface (D_{84} as in Recking et al., 2016), instead of the 50th percentile of the sediments on the riverbed surface (D_{50} in Eq. 11). They concluded that the choice of the characteristic diameter depends on the geomorphological context of the stream. In particular, for a "colluvial" stream pattern, as is the case for the Guerbe River, the use of the $D_{84,TraBL}$ yielded better model predictions than the D_{84}. Since in our work, we can only measure the grain size distribution representing the riverbed surface, we considered the D_{50} as representing the $D_{84,TraBL}$. We propose that this assumption is acceptable for the Guerbe River since streams with a "colluvial" pattern are characterized by similar D_{50} and $D_{84,TraBL}$ values (see Fig. 4 in Rickenmann and Fritschi, 2010 for the Erlenbach stream in the Swiss Alps and Fig. 7 in Piton and Recking, 2017 for the Upper Roize stream).

In summary, both the Meyer-Peter and Müller (1948), here referred to as MP.M, and Recking et al. (2016) formulations require the same key parameters to calculate the transported bedload, which are: the alluvial slope, the $D_{50,}$ and D_{84} grain size percentiles, the channel width, and water discharge.

3.3. Data acquisition

3.3.1. Uncrewed aerial vehicle (UAV) surveys and photogrammetry processing

We applied a UAV close-range setup in August-September 2021 to measure grain sizes on emerged gravel bars along the Guerbe River (Figs. 1b and 1c). We designed our surveys (13) and photogrammetric processing based on the workflow of Mair et al. (2022) with the aim of reducing the uncertainties related to the survey in the field and the processing of the data on the resulting grain sizes. To ensure a sufficient ground sampling distance of < 2 mm/pix in all pictures, we conducted close-range surveys with a nominal flight altitude between 5 and 9 m above ground. For image acquisition, we used a one-level grid of nadir camera positions as backbone geometry, for which we targeted a lateral and frontal overlap between individual images of 80%. We complemented this grid with images (5 to 20 per site) taken with oblique angles with a pitch of >20˚. The images were taken at the same survey altitude in an effort to minimize systematic errors during the photogrammetric processing (James and Robinson, 2014; Carbonneaun and Dietrich, 2017; James et al. 2020). All images were taken in the JPEG format with a DJI Mavic 2 Pro on-board camera (Hasselblad L1D-20c), which utilizes a global shutter. For referencing, we distributed 5 to 10 ground control points (GCPs) over each target gravel bars and measured them with a Leica Zeno GG04 Plus GNSS antenna with the real-time online Swipos-GIS/GEO RTK correction. This setup yields a horizontal precision of 2 cm and a vertical precision of 4 cm (2σ) under ideal conditions (Swisstopo, 2022). The subsequent photogrammetric processing followed standard structure from motion (SfM) workflows (e.g., James and Robson, 2012; Fonstad et al., 2013, Eltner et al., 2016) including recent updates (e.g., James et al, 2017a, b; 2020) to produce high quality orthomosaic and digital surface models (DSMs) for each gravel bar (e.g. Fig. S1). To do so, we used the Agisoft Metashape (v1.6 Pro) software, licensed to the Institute of Geological Sciences, University of Bern. In total, we processed 13 SfM models, with average checkpoint/GCP precision of 26.69 ± 17.72 mm and systematic errors < 10 cm (Table S1).

3.3.2. Grain size measurements

We manually measured the size of grains on the orthomosaics that resulted from the field surveys (see section above) by applying the approach of Woman (1954). Here we used the QGIS 3.22 open-source software to create a grid with a 0.5 m-wide spacing and to measure the sizes of grains. For each grain underneath a grid intersection, we measured the lengths of the a- and b-axes by fixing four dots at the grains' edges, thereby using these to define the two perpendicular axes (e.g. Fig. S1 and S2 in appendix). Because of the limited resolution of the images (Table S1 for image resolution), we defined a grain size measurement threshold of 2 cm. Accordingly, all grains smaller than this threshold were considered as equal to 2 cm. This consideration had no effect on our values of 50th or 84th grain size percentiles since the proportion of grains smaller than 2 cm was never larger than 25%. We then calculated the 50th and 84th percentile values from the grain size dataset to characterize each gravel bar. Following Mair et al. (2022), we estimated the related 95% confidence intervals using a combined bootstrapping and Monte Carlo modelling approach for which we employed the survey-specific SfM uncertainties (Table S1). Here, we assumed that the grains on the gravel bars are characteristic of

the material that was transported during equal mobility conditions since during these events the surveyed bars were flooded.

3.3.3. Topographic gradients and river widths

In the Guerbe River, the bedload transport is currently conditioned by the values of the engineered slopes (S_c in Fig. 3), which we measured from the DSMs obtained from the UAV images (Section 3.3.1). For non-engineered conditions, we inferred that the corresponding slopes (S_n in Fig. 3) would have been similar to the gradient of a 300 m-long reach around the site of interest where grain size data was collected (150 m upstream and 150m downstream), considering an elevation difference between at least 6 check dams. Here we used the LIDAR DEM swissALTI3D (swisstopo, 2019) with a spatial resolution of 0.5 m^2 as a basis. The slope values were then calculated by taking the difference in the topography of two points in the water flow direction and dividing this value by the distance between them. For each survey site, we repeated such measurements at least 30 times to calculate the 95% confidence interval of the slope. Also at these sites, we measured the active river's width on orthoimages (SWISSIMAGE, spatial resolution of 10 cm; swisstopo). We determined the cross-sectional stream widths by measuring the width of the check dams' spillways downstream of our survey reach, which is considered to represent the engineered river width during flood stages.

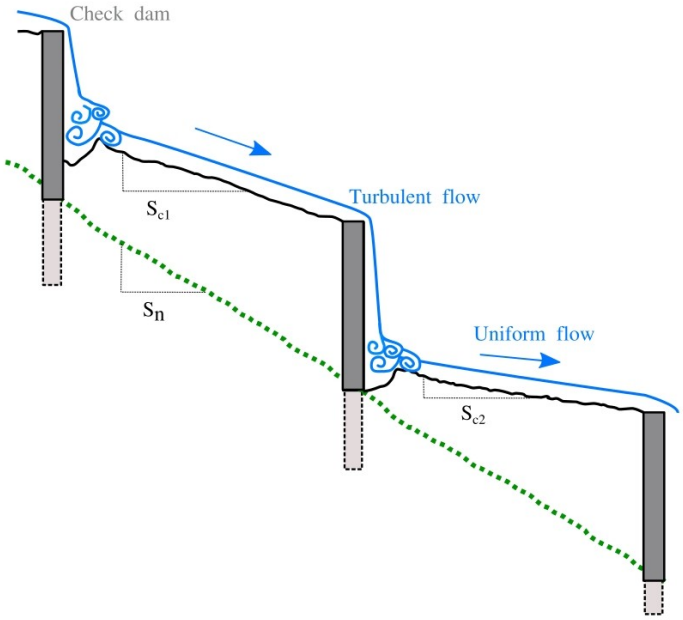

Figure 3. Topographic gradient along a reach between check dams: From the engineered riverbed (black line) we calculated the engineered slope of the river (S_c). Likewise, we calculated the non-engineered slope (S_n, green dashed line) using a 300 m-long reach around the site of interest.

3.3.4. Surface runoff

The water discharge is a further key parameter for calculating the sediment bedload flux (Eq. 1 to 11). The runoff can greatly vary over a short time interval, and such variations are even stronger during the entrainment of sediment particles in mountain streams (Tuset et al., 2016). This implies that information on the local runoff is necessary to properly calculate the rates of bedload transport. Here, we used the gauging records at Burgistein (Fig. 1a) as a reference, where sensors have measured the water levels every minute since 2009. These values have then been converted to water discharge based on an empirical relationship in which the related parameters were acquired at Burgistein (Spreafico and Weingartner, 2005). This station has been operated by the Bau- und Verkehrsdirektion des Kantons Bern (https://www.bvd.be.ch/), which offered us the water discharge data acquired between 2009 to 2021.

Since our area of interest is situated upstream of the Burgstein station (Fig. 1a), we downscaled the runoff values measured at Burgistein (Q_b) for our sites of interest (Q_l) by a factor that depends on the ratio between the size of the upstream catchment of the selected site (A_l) and that of the Burgistein station (A_b). This value was then multiplied by the ratio between the mean annual precipitation rate for the corresponding catchment contributing to water runoff at the selected site (P_l) and the Burgistein station (P_b):

$$Q_l = \frac{A_l}{A_b} \cdot \frac{P_l}{P_b} \cdot Q_b \tag{12}$$

Here, we employed an annual precipitation rate value of P_l = 1734 mm for our study reach and P_b = 1492 mm for the basin (Ramirez et al., 2022), which contributes to the runoff at Burgistein. We then used the gauging data collected over the past 12 years, based on which we estimated the range of bedload flux and also the total volume of sediment transported during this time, and we did so for engineered and non-engineered conditions in the Guerbe River. We acknowledge that this formulation deviates from the conventional method for estimating discharge at ungauged sites, which typically involves applying a power exponent to the catchment area ratio (McMahon et al., 2002). Given the wide range of values for this exponent, we opt for the use of the precipitation ratio. This ratio is grounded in data specific to our catchment and produces similar results as when applying a power exponent with values within the range of 0.9 to 0.95. We also acknowledge that the estimation of runoff upstream of a gauging station depends on multiple factors such as the groundwater level, the type of vegetation, and the thickness of the soil (Sriwongsitanon and Taesombat, 2011). However, since our gauging station is only c. 4 km downstream of our area of interest, we inferred that neglecting these factors will not significantly bias our estimations of the local runoff values.

3.3.5. Propagation of uncertainties in estimating the bedload flux

We applied a workflow that uses Monte Carlo simulation and bootstrapping to estimate the uncertainties of the bedload predictions (see S2 for a detailed description of the workflow). We proceeded through using the uncertainties that occur upon measuring the values of the key variables as input parameters, and through fitting the gamma distributions for the range of uncertainties that are associated with the percentiles

of the grain size datasets (i.e., the 95% CI on the D_{50} and D_{84}). These were obtained with the method proposed by Mair et al. (2022) to simulate the related uncertainties. The scale and shape parameters of the gamma distributions that we employed for the Monte Carlo simulation are presented in Table S3. We used normal distributions for all engineered and non-engineered slopes, with the standard deviation calculated from the 95% confidence interval divided by 4. For estimating the uncertainties on the width values we applied a uniform distribution where the length of this distribution was defined using the measured width including a ± 10% uncertainty at each site.

3.4. Considerations of non-engineered scenarios

For the non-engineered scenarios, we considered changes not only in the slope but also in the river width and grain sizes. In particular, in a natural state, the channel widths are expected to be smaller than the widths of the check dams' spillways as is currently the case. This has been shown in various engineered mountainous streams (Piton et al., 2017; Lucas-Borja et al., 2021) and is likely also valid for the Guerbe torrent. However, predictions of natural channel widths can be challenging because the hillslope instabilities around the channel can strongly affect this parameter, and information on widths was not available for the time before the check dams in the Guerbe River were constructed. Therefore, we had to make assumptions and considered three scenarios in which the current widths were shortened by 75%, 50% and 25%. Although we lack constraints to sustain these inferences, we justify the selection of these values because upstream of site 1 where the Guerbe River is poorly engineered, the channel widths are generally narrower than the width values we get when applying a 50% shortening. In the same sense, a prediction of grain size patterns for non-engineered conditions is speculative because of a lack of observations. Here, we used the grain size values from the bulk material upstream of site 1, which we considered as characterizing the source signal. Indeed, mapping shows that the highly active hillslopes just upstream of site 1 have most likely been the primary material source (Figs. 1a and 2). Furthermore, because riverbed grain sizes can also be affected by abrasion during transport in mountainous torrents (Miller et al., 2014), predictions about how the calibre of the bedload material changes downstream are almost impossible to make particularly for non-engineered states in the past. Therefore, we considered the grain sizes of the inferred supply signal as maximum values, which we kept as a constant parameter along the surveyed sites for some scenarios. Consequently, the non-engineered scenarios presented in this work will base on conservative assignments of values to the parameters, which control the transport of bedload material.

4. Results

4.1 Grain size, channel slope and width, and water discharge

We obtained data on bed surface grain sizes and channel slopes for engineered and non-engineered conditions for all 13 surveyed sites (Fig. 4). The D_{50} values resulting from the measurements show a decreasing trend from c. 8.3 cm to 2.4 cm in the downstream direction (Fig. 4a). In contrast, the sizes of the D_{84} rapidly decay between sites 1 and 2 from > 25 cm to < 20 cm, after which the values fluctuate between c. 20 and 10 cm (Fig. 4b). The measured slopes for engineered conditions display a similar pattern as the D_{84} in the sense that the energy gradient rapidly decreases from c. 10 to 5 cm m^{-1} between sites 1 and 2. The gradients then oscillate

around a value of c. 3 cm m^{-1} farther downstream (Fig. 4c). This pattern of alternating slope values is clearly visible for the reaches between all check dams in the dataset obtained from the 0.5 m SwissAlti3D DEM where the data collection was achieved in 2019 (Fig. S3). The non-engineered slopes are substantially different. They are flattest at site 1 and along the downstream portion of the fan (from site 7 onwards) where the values are c. 10 cm m^{-1} and less (Fig. 4d). In-between, the energy gradients continuously decrease in the downstream direction, starting with c. 20 cm m^{-1} at site 2 and ending with a value of 10 cm m^{-1} on the fan itself (Fig. 4d). This rapid increase in energy gradient between sites 1 and 2 points to the occurrence of a knickpoint in the longitudinal stream profile (see section 5.3 for more details), which is also corroborated by the geomorphological map where several break-in-slopes are visible on the hillslopes bordering the channel system in this area (Fig. 2). The current channel widths (thus during engineered conditions) fluctuate around a value of 15 m without displaying a clear trend in the downstream direction (Table S2). Please see Figures 4e, 7e and 8e for illustrations of the elevation profile and the locations of all surveyed sites.

The pattern of water discharge along the surveyed reach was calculated using Eq. 12 and the records at the Burgistein gauging station as a basis (Figs. S4). Accordingly, at the fan apex, the annual peak discharge values vary between 5 and 18 $m^3 s^{-1}$ (Fig. 5). Note that the latter value was registered in 2021 and has been the largest discharge during the surveyed period.

4.2 Bedload flux for engineered and non-engineered scenarios

We calculated the volumes of the instantaneous and mean annual bedload that can be transported along the surveyed sites by applying the MP.M. and Recking formula. Considering the constraints as elaborated in sections 3.4 and 4.1, the results show that for the engineered conditions, the mean annual bedload transport rate at the fan apex ranges from c. 1'000 to 6'000 $m^3 yr^{-1}$ if the MP.M. equation is used, or from 900 to 2'500 $m^3 yr^{-1}$ if the calculations are done with the Recking approach (Fig. 6). For the non-engineered state, we calculated mean annual transport rates that are between c. 10 (Recking formula) and 100 times higher (MP.M. formula). More specifically, the values for bedload transport at the apex vary from 30'000 to 400'000 $m^3 yr^{-1}$ using MP.M.'s equation for all scenarios of channel width shortening and grain sizes (Fig. 6a). Alternatively, the values are smaller if estimated with the Recking equation, and they vary between 1'000 to 150'000 $m^3 yr^{-1}$ (Fig. 6b). See a detailed discussion on these differences in section 5.1.

Along the segment upstream of the apex, the mean annual bedload fluxes calculated for all surveyed sites revealed specific patterns both for engineered and non-engineered conditions and also for the MP.M. and Recking approaches (Fig. 7). For the engineered conditions the use of the MP.M. equation predicts the highest bedload flux, which is c. 10'000 $m^3 yr^{-1}$ for site 1, whereas the fluxes are less than 2'500 $m^3 yr^{-1}$ for all the other surveyed sites (Fig. 7a). In contrast, the application of the Recking equation returns values of mean annual bedload flux that are less than 1'000 $m^3 yr^{-1}$ for all sites upstream of the fan apex (Fig. 7c). For the non-engineered conditions, the application of the MP.M. equation shows a rapid increase in the bedload capacity between sites 1 and 2, after which the values fluctuate around c. 400'000 $m^3 yr^{-1}$ in the downstream direction until the fan apex (Fig. 7b). In contrast, the application of the Recking approach predicts that sediment flux

continuously increases from < 1'000 m^3 yr^{-1} in the headwaters to > 60'000 m^3 yr^{-1} near the fan apex (Fig. 7d). If the stream's response to peak discharge conditions is considered, then for engineered conditions the MP.M. equation returns a peak sediment flux at site 1 of 0.3 $m^s s^{-1}$, after which the bedload flux fluctuates around a constant value that is c. 3 times lower than at site 1 (Fig. 8a). The pattern is similar if the Recking equation is used, but the values are generally 50% lower (Fig. 8c). In addition, also using the Recking equation, site 1 has a predicted sediment flux that is the same as farther downstream. If the non-engineered states are considered, then the application of the MP.M and Recking equations show both the same pattern for the peak discharge scenarios, where the bedload fluxes during peak discharge are between 8 (MP.M equation) and 20 times higher (Recking equation) than for engineered conditions (Figs. 8b and 8d).

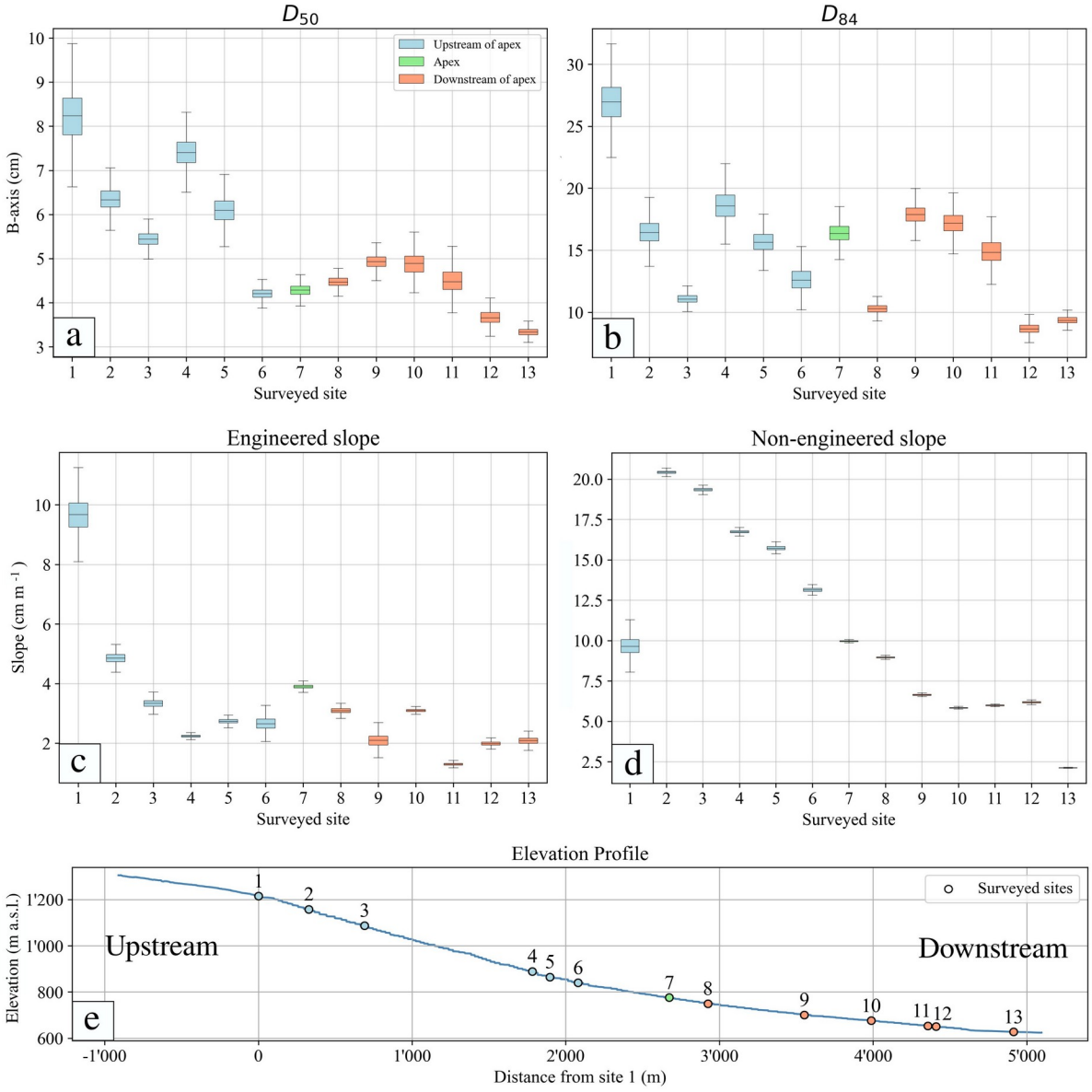

Figure 4. Boxplots representing the measured parameters at the surveyed sites with propagated uncertainties: (a) Bed surface grain size D_{50}, (b) size of the D_{84} of the sediments on the bed surface, (c) alluvial slope for the

engineered conditions, and (d) alluvial slope obtained from the DEM for non-engineered conditions. (e)
446 Elevation profile of the Guerbe River. The sites upstream and downstream of the alluvial fan's apex are indicated by the blue and red colours, respectively, and the site on the apex is indicated by the green colour.

448

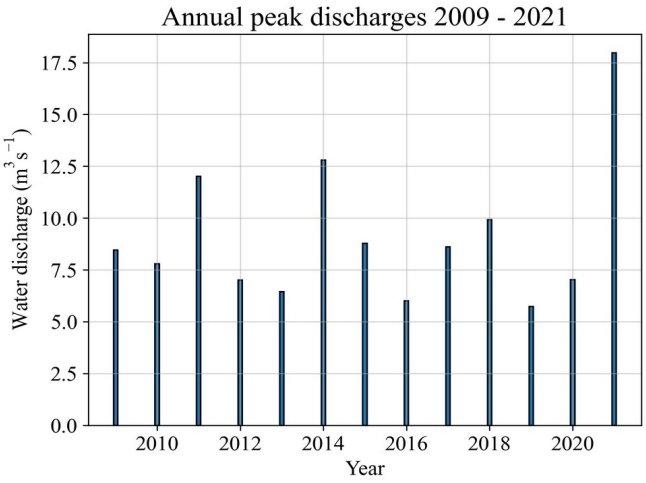

450 **Figure 5.** Calculated values of annual peak discharge for the fan apex of the alluvial fan in the Guerbe River during the period between 2009 and 2021.

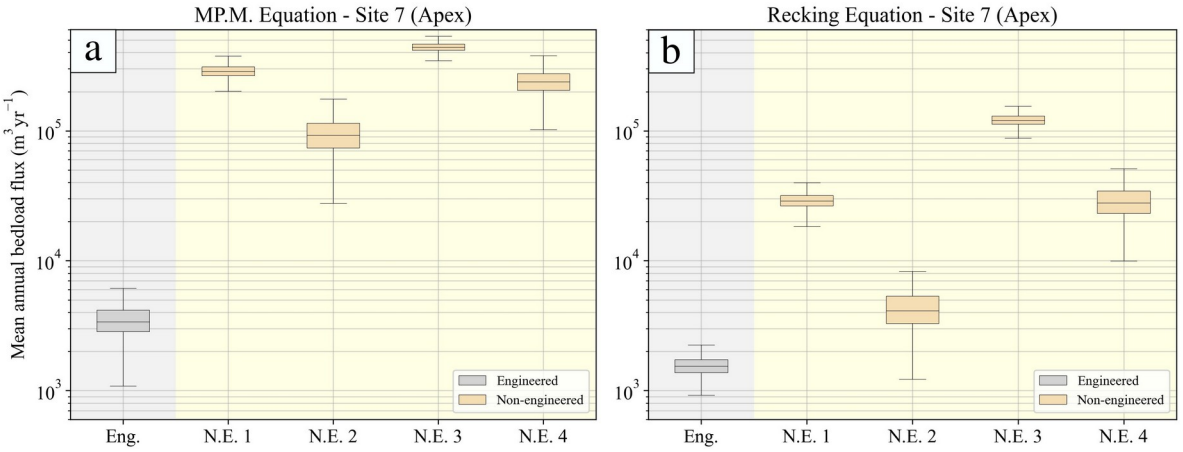

452 **Figure 6.** Boxplot representation of the mean annual bedload estimates using (a) the MP.M. and (b) the Recking approaches for the Guerbe River catchment. The engineered (Eng.) and the non-engineered (N.E.) scenarios are
454 based on using the parameters shown in Fig. 4. Specifically, the engineered scenario is based on the average of the engineered slopes, whereas the results for the non-engineered scenarios are based on: (N.E.1) a 75%
456 reduction of the channel width and grain sizes from site 7; (N.E. 2) a 75% reduction of the channel width and

grain sizes from site 1; (N.E. 3) a 25% reduction of the channel width and grain sizes from site 7; and (N.E. 4) 25% reduction of the channel width and grain sizes from site 1.

Downstream of the apex, the two equations yield the same pattern where both the peak and mean annual bedload fluxes have lower values than at the apex for non-engineered conditions (Figs. 7 and 8). Yet, for the engineered conditions, we observed that the flux pattern locally reached high values particularly if the Recking equation is applied. Finally, to identify potential locations of riverbed armour breaking during peak discharge, we estimated the bedload flux by applying the Shields equation (Eq. 4) with the D_{84} grain size as a threshold (Schlunegger et al., 2020). This estimation is a variation of the result presented in Fig. 8 for the peak discharge in 2021, where we considered armour breaking if the calculated bedload flux exceeds 0.001 $m^3\ s^{-1}$ (Table S4). When armour breaking occurs, we anticipate a substantial material transport and expect changes in the channel morphology, including slope variations, during and after the event. Under engineered conditions, our results suggest that such channel bedform reorganization might occur at only a few specific sites (Table S4). Conversely, in a non-engineered scenario, almost all sites are predicted to experience armor-breaking conditions during a flood with a magnitude comparable to the 2021 peak discharge (Table S4).

5. Discussion

The application of two different approaches to calculate the bedload transport capacity revealed specific differences, which become more important when considering the non-engineered status. In contrast, where bedload transport rates are calculated for engineered conditions, the differences resulting from the two formulations are less and within uncertainties. This will further be discussed in section 5.1. Thereafter, we discuss how the check dams potentially contribute to the regulation of sediment transport (section 5.2) and how the stabilization of the channel bed affects the consolidation of the hillslopes (section 5.3).

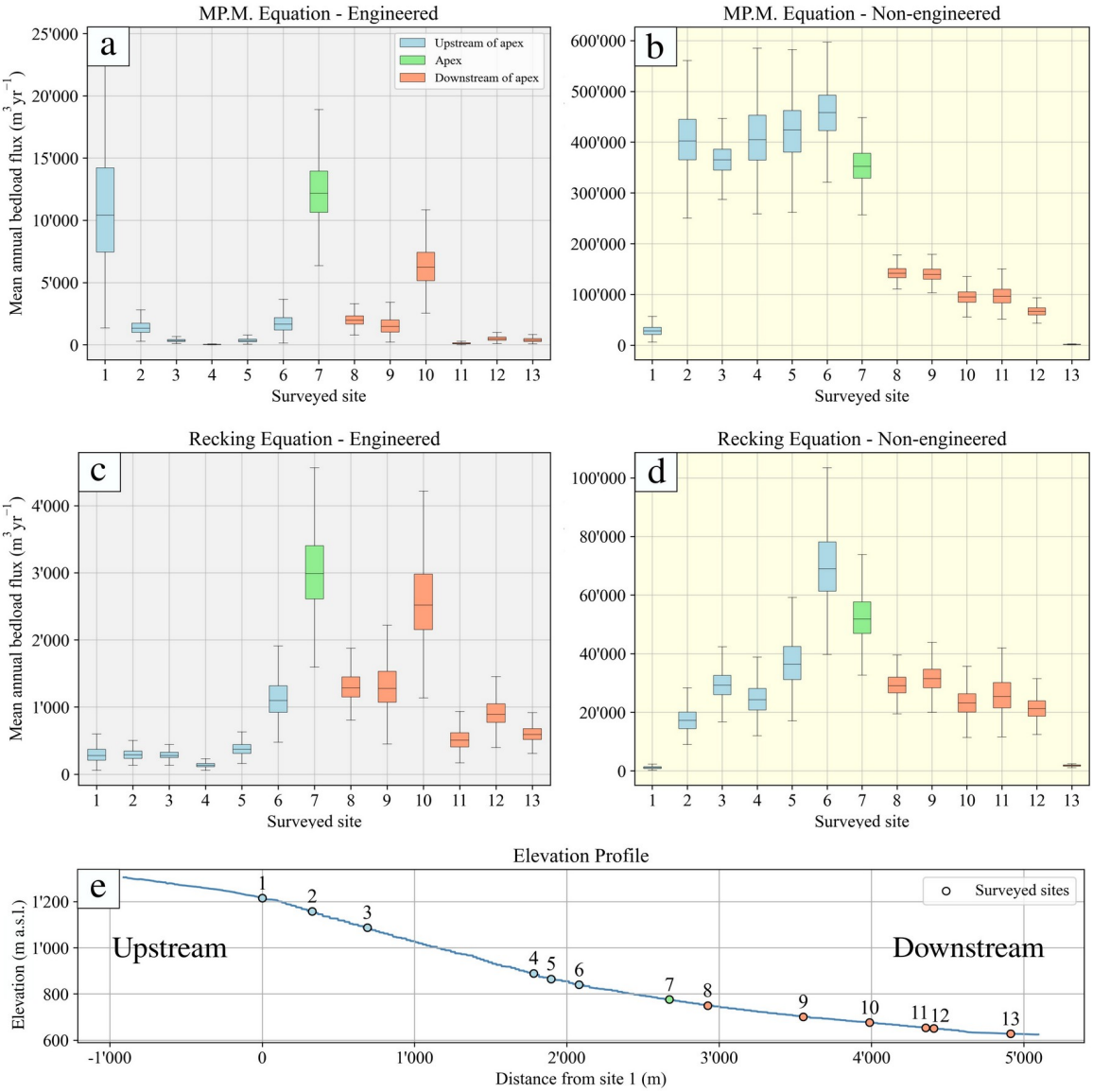

478 **Figure 7.** Boxplot representation of the annual mean bedload estimates using the MP.M. and the Recking along all the surveyed sites. For the values of the parameters to compute the sediment flux for engineered (a and c) and
480 non-engineered (b and d) scenarios, please refer to Fig. 4. Specifically, the non-engineered scenario is based on the assumption that the width of the channel is reduced by 50%. The sites upstream and downstream of the
482 alluvial fan apex are indicated by the blue and red colours, respectively, and the site on the apex is indicated by the green colour.

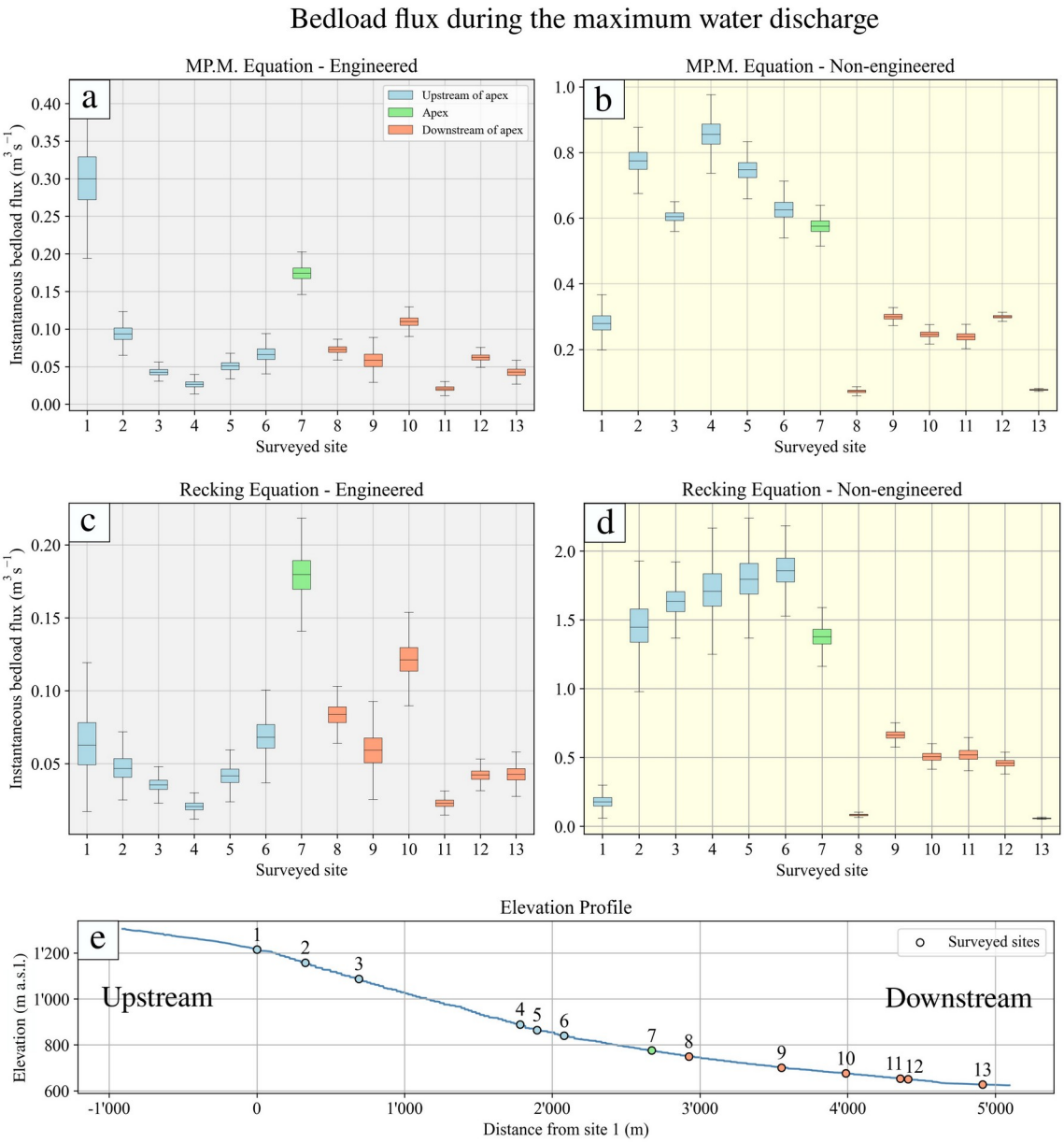

484 **Figure 8.** Boxplot representation of the bedload predictions using MP.M. and Recking during the 2021 peak runoff along all the surveyed sites. The engineered (a and c) and the non-engineered (b and d) scenarios are
486 based on the parameters shown in Fig. 4. Specifically, in the non-engineered scenario we show the results where 50% of the current channel width is employed. The sites upstream and downstream of the alluvial fan apex are
488 indicated by the blue and red colours, respectively, and the site on the apex is indicated by the green colour.

5.1. Analysis of the equations' results

490 For non-engineered conditions, we consider the MP.M. approach to yield a strong overestimation of the mean annual sediment bedload flux if the results of the Recking equation are taken as a reference. We justify the
492 selection of this benchmark because the Recking formula was explicitly validated with data from steep mountainous catchments such as the Guerbe River (see above). Furthermore, a recently published dataset on

494 sediment load in torrent catchments reveals that for areas below 5 km^2, the maximum sediment supply is approximately 13'000 m^3 yr^{-1} (Morel et al., 2023). Similar to the Guerbe case, this value is of the same order of
496 magnitude as the predictions by the Recking equation (N.E. 1 and N.E. 4 in Fig. 6b) and is roughly 10 times less than the predictions from the MP.M. for a non-engineered situation (Fig. 6a). This overestimation of the bedload
498 transport rates mainly concerns the cases of low water discharge (Fig. 9b). Because low water fluxes occur more frequently during one year than peak discharges, the mean annual bedload transport rates will be higher. For
500 peak discharges, however, the Recking equation predicts much higher sediment fluxes than the MP.M. equation (Fig. 9b). Since the Recking approach was also validated for peak water flux (see above), we consider the
502 resulting values for the Guerbe River as realistic. For the engineered conditions, however, both equations predict similar sediment fluxes during low and high runoff (Fig. 9a), thereby explaining why predictions of mean
504 annual sediment fluxes are nearly the same for both equations.

We also compare our outcomes with two available studies in the Guerbe catchment. The first one
506 estimated the sediment budget from ^{10}Be concentrations in the catchment (Delunel et al., 2020), where a denudation rate of approximately 260 mm kyr^{-1} on our surveyed catchment area gives a mean annual sediment
508 yield of c. 3'000 m^3 yr^{-1}. Conventionally, cosmogenic data integrate denudation of times scales of several thousands of years (von Blanckenburg, 2005) and as such this value would correspond to the total sediment flux
510 prior to the construction of the check dams. However, as will be argued below, the construction of these steps resulted in a partial disconnection between the shallow-seated landslides and the Guerbe River particularly
512 along the margin of the trunk channel (e.g. the Riselbruch landslide which became stabilized after the check dams were built, see section 5.3). Because the foot of a landslide has been documented to release material with
514 low ^{10}Be concentrations (Cruz Nuñes et al., 2015), we anticipate that during pre-engineered conditions the concentrations of cosmogenic ^{10}Be in riverine quartz would have been lower. Therefore, we consider the
516 sediment flux of the c. 3'000 m^3 yr^{-1} as representative of the current state. The second study used the CEASAR-Lisflood evolution model to estimate the total sediment load (suspended and bedload) for engineered conditions,
518 where a mean annual sediment load of 1'222 m^3 yr^{-1} was predicted (Ramirez et al., 2022). Both results can be converted to mean annual bedload fluxes by applying a 60% factor, based on the results of sediment budgets
520 carried out on mountain streams in the Alps for basins that are c. 10 km^2 large (Schlunegger and Hinderer, 2003). Therefore, applying these corrections for the current engineered state, the ^{10}Be-based bedload flux is c.
522 1'800 m^3 yr^{-1}, whereas the related value derived with the CEASAR-Lisflood evolution model would be in the range of c. 700 m^3 yr^{-1}. Considering the uncertainties that are associated with estimating bedload transport, the
524 cosmo-based sediment flux and the estimates by Ramirez et al. (2022) are in agreement with the outcome of our calculations based on the Recking formula.

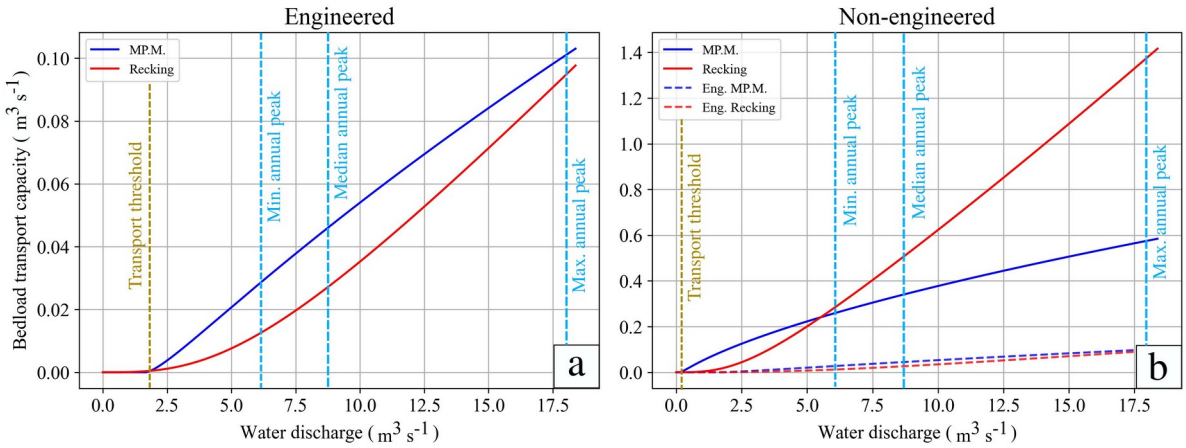

Figure 9. Predicted bedload versus water discharge patterns using the MP.M and Recking approaches for (a) engineered and (b) non-engineered conditions. These patterns were determined using data collected at site 7 (Fig. 4). Specifically, as shown in this figure, the results for the engineered scenario are based on the average of the engineered slopes. Those of the non-engineered scenario considered a 50% reduction of the channel width at site 7, and the grain size data that was also collected at that site.

5.2. Regulation of sediment transport

For engineered conditions and considering the last peak water discharge event in 2021, the predictions using the MP.M. and Recking approaches reveal site-specific fluctuations in both the transport capacity and the armour-breaking probability (Fig. 8 and Table S4). This pattern suggests that sediment transport is regulated through buffering effects where during a peak discharge event some sites will store a fraction of the supplied sediment while others will release a large portion of the previously stored material. Such regulation has already been described for filled check dams where the concrete structures (such as check dams) create fixed points along a longitudinal profile of a river, which disconnects the reaches between the dams (Piton et al., 2017). In addition, check dams reduce the length of the reach where spontaneous erosion could occur, thereby reducing the risk where large volumes of sediment are released and transported downstream in a short time (Piton and Recking, 2016). We consider that the occurrence of such a regulation is recorded by the downstream fluctuations of the alluvial slopes (Figure 4 and S3) where segments with flat slopes have the potential to store further material, whereas reaches with steep slopes will likely represent a sediment source during a next event when large water fluxes occur. As an additional consequence of such a regulation, the grain size will rapidly fine downstream through selective transport, particularly along the depositional sites. Such a mechanism was predicted by theory (Paola et al., 1992) and is documented by our data (Fig. 4). Note, however, that besides selective transport, the breaking of grains as they fall from the dams into the pool likely also contributes to the fining of the material (Miller et al., 2014).

5.3. Bed stabilization and hillslope consolidation

We interpret that the check dams contribute effectively to the bed stabilization of the Guerbe River (Piton et al., 2017; Lucas-Borja et al., 2021). We infer the occurrence of such a mechanism at work using the results of the MP.M. and Recking equations, both of which predict that in the absence of check dams, the mean annual transport capacity would be substantially higher. This is particularly true along the segment between sites 1 and 2 when the predictions of the sediment flux for the non-engineered state is compared to the flux values characterizing the engineered conditions (Fig. 7b and 7d). This is also the region where we mapped a major knickzone on the hillslopes that border the channel network (Fig. 2). Such features are usually considered as evidence for the occurrence of high surface erosion and sediment production rates (Van den Berg and Schlunegger, 2012; Whittaker and Boulton, 2012; Battista et al., 2020), and they would most likely represent the sites of major sediment production in the case that no check dams had been built. It appears that the check dams are stabilizing the bed, thereby reducing the erosional potential along the reach, which otherwise would be an important sediment factory.

In a scenario where the Guerbe riverbed has not been stabilized, fluvial erosion could lead to an increase in sediment supply by activating shallow-seated landslides (Piton et al., 2017; Lucas-Borja et al., 2021). Such a mechanism at work has been documented for the Erlenbach River, which is an Alpine torrent in Central Switzerland (Rickenmann and Fritschi, 2010). For this basin, Molnar et al. (2010) documented an increase in the slip rates of landslides following a period of rapid fluvial dissection. For the case of the Guerbe basin, an inspection of satellite images taken between 1970 and the present from the Guerbe River discloses that between sites 1 and 2 the landslide activity in the Riselbruch (Knickpoint zone in Fig. 2, S5a and S5b) decreased after the construction of the check dams along this reach leading to a reforestation of the area (Fig. S5c and S5d). We use this example to argue that the check dams in the Guerbe River contribute to the consolidation of the hillslopes (Piton et al., 2017; Lucas-Borja et al., 2021). This mechanism results in a stabilisation of the terrain surrounding the channel, which allows the growth of a stable vegetation as the landsliding activities decrease. Furthermore, the application of the Recking equation predicts that in the absence of check dams, such a hillslope de-consolidation will not only occur in the uppermost area surrounding the knickzone but also along the entire reach upstream of the fan apex (Fig. 7d). We base this inference on the predicted downstream increase in the bedload sediment flux.

5.4. Are check dams really effective in reducing hazard impact?

From our results, we conclude that the presence of check dams in the Guerbe River does reduce the bedload flux outcoming from the sediment production area, thus reducing the potential for hazards in the downstream reaches of the stream. However, this conclusion is only valid if we assume that the check dams will not fail over time, which has indeed not been the case with the Guerbe River during the past hundreds of years (Salvisberg, 2017). In fact, Ramirez et al. (2022) showed that a failure of one or multiple check dams releases a large amount of the material that was originally stored behind the concrete structures. These authors also showed that such failure can initiate a cascade where other dams will break in the downstream direction. It is

possible that re-activations of deep-seated landslides can initiate such a failure. Recently, the displacement of
588 the deep-seated Meierisli landslide has damaged >10 of these structures (Andres and Badoux, 2019), with the consequence that some of them are likely to break and thus to fail in the next years. It was also found by the
590 responsible engineers (G. Hunziker, pers. comm. 2022) that the slip of such landslides has not been influenced by the presence of check dams during the past decades, with the consequence that they have constantly applied
592 lateral stress on the concrete structure, causing them to eventually break. Consequently, in order to guarantee the functioning of the check dams as we described above, it is necessary that such infrastructure will be
594 continuously maintained and repaired after some damages, and that the deep landslides will eventually be surveyed and engineered if possible. From a broader perspective, the results of our study can be extended to
596 other steep mountain streams that have already been managed with such infrastructure. In addition, we propose that the outcome of our analysis might be used as guidelines for projects that aim at building a staircase system
598 along a steep mountainous stream.

6. Conclusions

600 The analysis presented above shows that the current presence of check dams in a steep alpine stream (Guerbe River) has a major influence on mitigating the sediment production in the catchment and, consequently,
602 reducing the risks of hazards related to high sediment fluxes. We applied two different approaches to calculate bedload fluxes, which were based on the Meyer-Peter and Müller (MP.M.) and the Recking equation, and we
604 applied them for engineered and non-engineered conditions. Both equations resulted in similar predictions regarding mean annual bedload fluxes for the currently engineered state, and they also predict higher transport
606 rates of bedload material for the non-engineered state. However, models that are based on the Recking solution predict an increase in bedload flux for non-engineered conditions that is c. 10 times higher than for the
608 engineered state, whereas the MP.M. equation predicts a bedload flux that is even 100 times larger. Since the Recking approach was calibrated with data from mountain streams with a channel floor morphology
610 characterized by steps and pools, we consider the resulting predictions for non-engineered scenarios as more reliable than those derived from the MP.M. formula. Importantly, we find that the check dams regulate sediment
612 transport through buffering pulses of sediment during high discharge conditions. In particular, reaches separated by check dams can either function as a sedimentary sink or as a material source. This is observed by the
614 downstream variations of local energy gradients where segments with a higher slope could potentially act as a sediment source, whereas reaches with flatter slopes have the potential to store some of the supplied material.
616 As a second function, we considered that check dams contributed to the stabilization of the channel bed. We infer this by our model results, particularly for the uppermost region where check dams were built. There, for
618 non-engineered conditions, the models predict a large increase in the bedload transport rate where the slope rapidly increases downstream of a knickpoint, as would be expected for a reach characterized by a knickpoint
620 retreat. For engineered conditions, however, our models predict that the transport rates of bedload material remain stable despite the occurrence of a knickpoint. As a consequence, the retreat of this particular knickpoint
622 will not occur as long as the check dams are in operation. Finally, we infer that check dams also contribute to the stabilization of the bordering hillslopes, mainly because they prevent the stream from incising into the

substratum. Therefore, we conclude that our approach is a useful and promising tool to evaluate the first-order efficiency of check dams in reducing bedload sediment flux in steep mountain streams.

Notation

The following symbols are used in this paper:

A	catchment area (m^2);
D_{50}	sediment diameter such that 50 % of the bed surface mixture is finer grained (m);
D_{84}	sediment diameter such that 84 % of the bed surface mixture is finer grained (m);
Φ	dimensionless Einstein parameter;
g	gravity acceleration ($m\ s^{-2}$)
Q_s	bedload ($m^3\ s^{-1}$);
q	unit water discharge ($m^2\ s^{-1}$);
Q	water discharge ($m^3\ s^{-1}$);
ρ_s	sediment density (2600 kg m^{-3});
ρ_w	water density (1000 kg m^{-3});
S	Energy gradient ($m\ m^{-1}$);
τ^*	dimensionless shear stress;
τ_c^*	Shields number (dimensionless);
τ_m^*	Recking equation parameter (dimensionless);
τ	shear stress ($N\ m^{-2}$);
v	mean water velocity in depth ($m\ s^{-1}$);
W	channel width (m).

Acknowledgments. The authors are grateful for the Bau- und Verkehrsdirektion des Kantons Bern (https://www.bvd.be.ch/), which kindly offered us the water discharge for the Guerbe River. We greatly appreciate that the SWISSTOPO made the DEMs and images available at no costs.

Financial support. This research has been supported by the University of Bern and Innovative Training Network S2S (grant no. 860383).

Author contributions. AHdP, DM, PG and FS applied the UAV close-range setup in the Guerbe River. DM designed the UAV close-range setup applied in this work. AHdP measured the grain sizes and performed the analyses described in this paper. AHdP wrote the manuscript with support from DM, PG, CS, ACW, SC and FS.

Competing interests. The contact author has declared that neither they nor their co-authors have any competing interests.

References

Andres, N., and Badoux, A.: Unwetterschäden in der Schweiz im Jahre 2018. Rutschungen, Murgänge, Hochwasser und Sturzereignisse. Wasser, Energie, Luft, 111(1), 29-38, 2019.

Bagnold, R.A.: An empirical correlation of bedload transport rates in flumes and natural rivers. Proceedings of the Royal Society of London A372: 453–473, https://doi.org/10.1098/rspa.1980.0122, 1980.

Battista, G., Schlunegger, F., Burlando, P., and Molnar, P.: Modelling localized sources of sediment in mountain catchments for provenance studies. Earth Surf. Process. Landforms 45 (14), 3475–3487. https://doi.org/10.1002/esp.v45.1410.1002/esp.4979, 2020.

Bombino, G., Boix-Fayos, C., Gurnell, A.M., Tamburino, V., Zema, D.A., and Zimbone, S.M.: Check dam influence on vegetation species diversity in mountain torrents of the Mediterranean environment. Ecohydrology 7 (2), 678–691, https://doi.org/10.1002/eco.1389, 2014.

Carbonneau, P. E. and Dietrich, J. T.: Cost-effective nonmetric photogrammetry from consumer-grade sUAS: implications for direct georeferencing of structure from motion photogrammetry, Earth Surf. Proc. Land., 42, 473–486, https://doi.org/10.1002/esp.4012, 2017

Castillo, C., Perez, R., and Gomez, J.A.: A conceptual model of check dam hydraulics for gully control: efficiency, optimal spacing and relation with step-pools. Hydrol. Earth Syst. Sci 18, 1705–1721. http://dx.doi.org/10.5194/hess-18-1705-2014, 2014.

Cruz Nunes, F., Delunel, R., Schlunegger, F., Akçar, N., Kubik, P.W.: Bedrock bedding, landsliding and erosional budgets in the central European Alps. Terra Nova 27 (5), 370–378, https://doi.org/10.1111/ter.12169, 2015.

Delunel, R., Schlunegger, F., Valla, P.G., Dixon, J., Glotzbach, C., Hippe, K., Kober, F., Molliex, S., Norton, K.P., Salcher, B., Wittmann, H., Akçar, N., and Christl, M.: Late-Pleistocene Catchment-wide Denudation Patterns Across the European Alps. https://doi.org/10.1016/j.earscirev.2020.103407, 2020.

Einstein, H.A.: The Bed-load Function for Sediment Transportation in Open Channel Flows. United States Department of Agriculture Soil Conservation Service: Washington, DC; 71, 1950.

Eltner, A., Kaiser, A., Castillo, C., Rock, G., Neugirg, F., and Abellán, A.: Image-based surface reconstruction in geomorphometrymerits, limits and developments, Earth Surf. Dynam., 4, 359– 389, https://doi.org/10.5194/esurf-4-359-2016, 2016.

Ferguson, R.I.; Flow resistance equations for gravel- and boulder-bed streams. Water Resour. Res. 43, W05427. http://dx.doi.org/10.1029/2006WR005422, 2007.

Fonstad, M. A., Dietrich, J. T., Courville, B. C., Jensen, J. L., and Carbonneau, P. E.: Topographic structure from motion: A new development in photogrammetric measurement, Earth Surf. Proc. Land., 38, 421–430, https://doi.org/10.1002/esp.3366, 2013.

Jäckle, S.: Hydrologischer atlas der Schweiz. Wildbach gürbe gurni-geldwattenwil (Vol. 6.1). Berne, Schweiz: Geographisches Institut der Universität Bern, 2013.

James, M. R. and Robson, S.: Straightforward reconstruction of 3D surfaces and topography with a camera: Accuracy and geoscience application, J. Geophys. Res.-Earth, 117, F03017, https://doi.org/10.1029/2011JF002289, 2012.

James, M. R., and Robson, S.: Mitigating systematic error in topographic models derived from UAV and ground-based image networks, Earth Surf. Proc. Land., 39, 1413–1420, https://doi.org/10.1002/esp.3609, 2014.

James, M. R., Robson, S., and Smith, M. W.: 3-D uncertaintybased topographic change detection with structure-from-motion photogrammetry: precision maps for ground control and directly georeferenced surveys, Earth Surf. Proc. Land., 42, 1769–1788, https://doi.org/10.1002/esp.4125, 2017a.

James, M. R., Robson, S., d'Oleire-Oltmanns, S., and Niethammer, U.: Optimising UAV topographic surveys processed with structure-from-motion: Ground control quality, quantity and bundle adjustment, Geomorphology, 280, 51–66, https://doi.org/10.1016/j.geomorph.2016.11.021, 2017b.

James, M. R., Antoniazza, G., Robson, S., and Lane, S. N.: Mitigating systematic error in topographic models for geomorphic change detection: accuracy, precision and considerations beyond off-nadir imagery, Earth Surf. Proc. Land., 45, 2251–2271, https://doi.org/10.1002/esp.4878, 2020.

Julien, P. Y.: Erosion and Sedimentation. Cambridge Univ. Press 2, Cambridge, UK., 2010.

Kaitna, R., Chiari, M., Kerschbaumer, M., Kapeller, H., Zlatic-Jugovic, J., Hengl, M., and Huebl, J.: Physical and numerical modelling of a bedload deposition area for an Alpine torrent. Natural Hazards and Earth System Sciences, 11(6), 1589, https://doi.org/10.5194/nhess-11-1589-2011, 2011.

Karim, F., Kennedy, J.F.: Menu of couple velocity and sediment discharge relations for rivers. Journal of Hydraulic Engineering 116(8): 978-996, https://doi.org/10.1061/(ASCE)0733-9429(1990)116:8(978) , 1990.

Keiler, M., and Fuchs, S.: Challenges for natural hazard and risk management in mountain regions of Europe. In Oxford research encyclopedia of natural hazard science. Oxford, U.K.: Oxford University Press, https://doi.org/10.1093/acrefore/9780199389407.013.322, 2018.

Lamb MP, Dietrich WE, Venditti J-G.: Is the critical Shields stress for incipient sediment motion dependent on channel-bed slope? Journal of Geophysical Research 113: F02008, https://doi.org/10.1029/2007JF000831, 2008.

Lucas-Borja, M. E., Piton, G., Yu, Y., Castillo, C. & Antonio Zema, D. Check dams worldwide: objectives, functions, effectiveness and undesired effects. *Catena* 204, 105390, https://doi.org/10.1016/j.catena.2021.105390, 2021.

Mair, D., Do Prado, A.H., Garefalakis, P., Lechmann, A., Whittaker, A., and Schlunegger, F.: Grain size of fluvial gravel bars from close-range UAV imagery-uncertainty in P. Garefalakis, A.H. do Prado, D. Mair et al. Sedimentary Geology 446 (2023) 106340 21 segmentation-based data. Earth Surface Dynamics 10, 953–973, https://doi.org/10. 5194/esurf-2022-19, 2022.

McMahon, T.A., Fenton, J., Stewardson, M., Costelloe, J., and Finlayson, B.: Estimating discharge at an ungauged site. Australian Journal of Water Resources, 5, 113–117, https://doi.org/10.1080/13241583.2002.11465197, 2002.

Meyer-Peter, E., Mueller, R.: Formulas for bed-load transport. Proceedings, 2nd Meeting IAHR, Stockholm; 39–64, 1948.

Miller, K.L., Szabo, T., Jerolmack, D.J., and Domokos, G.: Quantifying the significance of abrasion and selective transport for downstream fluvial grain size evolution. J. Geophys. Res. 119, 2412–2429, https://doi.org/10.1002/2014JF003156, 2014.

Molnar, P., Densmore, A.L., McArdell, B.W., Turowski, J.M., and Burlando, P.: Analysis of changes in the step-pool morphology and channel profile of a steep mountain stream following a large flood. Geomorphology 124(1): 85–94, https://doi.org/10.1016/j.geomorph.2010.08.014, 2010.

Morel, M., Piton, G., Kuss, D., Evin, G., and Le Bouteiller, C.: Statistical modeling of sediment supply in torrent catchments of the northern French Alps, Nat. Hazards Earth Syst. Sci., 23, 1769–1787, https://doi.org/10.5194/nhess-23-1769-2023, 2023.

Paola, C., Parker, G., Seal, R., Sinha, S.K., Southard, S.K., and Wilcock, P.R.: Downstream fining by selective deposition in a laboratory flume, Science, 258(5089), 1757–1760, https://doi.org/10.1126/science.258.5089.1757, 1992.

Parker, G.: Transport of gravel and sediment mixtures, in: Sedimentation Engineering: Processes, Measurements, Modeling, and Practice. ASCE Manual 54. American Society of Civil Engineers (ASCE): Reston, VA xxi; 1132 pp, 2008.

Piton, G., and Recking, A.: Effects of check dams on bed-load transport and steep-slope stream morphodynamics. Geomorphology 291, 94–105, https://doi.org/10.1016/j.geomorph.2016.03.001, 2016.

Piton, G., and Recking, A.: The concept of 'travelling bedload' and its consequences for bedload computation in mountain streams, EarthSurface Processes and Landforms42(10): 1505–1519, https://doi.org/10.1002/esp.4105, 2017.

Piton, G., Carladous, S., Recking, A., Tacnet, J., Liebault, F., Kuss, D., Quefféléan, Y., and Marc, O.: Why do we build check dams in Alpine streams? An historical perspective from the French experience. Earth Surf. Process. Landf. 42, 91–108, https://doi.org/10.1002/esp.3967, 2017.

Ramirez, J.A., Mertin, M., Peleg, N., Horton, P., Skinner, C., Zimmermann, M., and Keiler, M.: Modelling the long-term geomorphic response to check dam failures in an alpine channel with CAESAR-Lisflood. Int. J. Sediment Res. http://dx.doi.org/10.1016/j.ijsrc.2022.04.005, 2022.

Recking, A.: Simple method for calculating reach-averaged bedload transport. Journal of Hydraulic Engineering 139: 70–75, https://doi.org/10.1061/(ASCE)HY.1943-7900.0000653, 2013.

Recking, A., Liébault, F., Peteuil, C., and Jolimet, T.: Testing bedload transport equations with consideration of time scales, Earth Surface Processes and Landforms 37(7): 774–789, https://doi.org/10.1002/esp.3213, 2012.

Recking, A., Piton, G., Vázquez-Tarrío, D., and Parker, G.: Quantifying the morphological print of bedload transport, Earth Surface Processes and Landforms 41(6): 809–822, https://doi.org/10.1002/esp.3869, 2016.

Rickenmann, D.: Comparison of bed load transport in torrents and gravel bed streams, Water Resources Research 37(12):3295–3305, https://doi.org/10.1029/2001WR000319, 2001.

Rickenmann, D., and Fritschi B.: Bedload transport measurements using piezoelectric impact sensors and geophones. In Bedload-surrogate monitoring technologies: U.S. Geological Survey Scientific Investigations Report 2010-5091, Gray JR, Laronne JB, Marr JDG (eds): Reston, VA.; 407–423, 2010.

Rickenmann, D., and Recking, A.: Evaluation of flow resistance in gravel-bed rivers through a large field dataset. Water Resources Research 47: 1–22, https://doi.org/10.1029/2010WR009793, 2011.

Salvisberg, M.: Die unzahmbare Gürbe: Überschwemmungen und hochwasserschutz seit dem 19. Jahrhundert. Basel, Schweiz: Schwabe AG, 2017.

Schlunegger, F., and Hinderer, M.: Pleistocene/Holocene climate change, reestablishment of fluvial drainage network and increase in relief in the Swiss Alps. Terra Nova 15 (2), 88–95, https://doi.org/10.1046/j.1365-3121.2003.00469.x, 2023.

Schlunegger, F., Delunel, R., and Garefalakis, P.: Short communication: Field data reveal that the transport probability of clasts in Peruvian and Swiss streams mainly depends on the sorting of the grains, Earth Surf. Dynam., 8, 717–728, https://doi.org/10.5194/esurf-8-717-2020, 2020.

Shields, A.: Application of similarity principles and turbulence research to bed load movement, SCSC Laboratory, California Institute of Technology, USDA, Pasadena, CA, 1936.

Shvidchenko, A., Pender, G., and Hoey, T.B.: Critical shear stress for incipient motion of sand/gravel streambeds. Water Resources Research 37(8): 2273, https://doi.org/10.1029/2000WR000036, 2001.

Spreafico, M., and Weingartner, R.: The hydrology of Switzerland. Selected aspects and results (Reports, Bundesamt f. Wasser u.Geologie (BWG) Water Series No. 7), 2005.

Sriwongsitanon, N., and Taesombat, W.: Effects of land cover on runoff coefficient, J. Hydrol. 410 (3–4), 226–238. http://dx.doi.org/10.1016/j.jhydrol.2011.09.021, 2011.

Swisstopo: Swiss Positioning Service swipos, https: //www.swisstopo.admin.ch/en/geodata/geoservices/swipos.html, last access: 26 February, 2022.

Tuset, J., Vericat, D., Batalla, R.: Rainfall, runoff and sediment transport in a Mediterranean mountainous catchment. Sci. Total Environ. 540, 114–132, https://doi.org/10.1016/j.scitotenv.2015.07.075, 2016.

Van den Berg, F., and Schlunegger, F.: Alluvial cover dynamics in response to floods of various magnitudes: The effect of the release of glaciogenic material in a Swiss Alpine catchment, Geomorphology, 141–142, 112–133, https://doi.org/10.1016/j.geomorph.2011.12.030, 2012.

von Blanckenburg, F.: The control mechanisms of erosion and weathering at basin scale from cosmogenic nuclides in river sediment. Earth and Planetary Science Letters 237: 462–479, https://doi.org/10.1016/j.epsl.2005.06.030, 2005.

Whittaker, A.C., Boulton, S.J.: Tectonic and climatic controls on knickpoint retreat rates and landscape response times. Journal of Geophysical Research 117, F02024, https://doi.org/10.1029/2011JF002157, 2012.

Wong, M., and Parker, G.: Re-analysis and correction of bed load relation of Meyer-Peter and Muller using their own database. Journal of Hydraulic Engineering 132(11): 1159–1168, https://doi.org/10.1061/(ASCE)0733-9429(2006)132:11(1159), 2006.

Wolman, M. G.: A method of sampling coarse riverbed material, Trans. Am. Geophys. Union, 35, 951, https://doi.org/10.1029/TR035i006p00951, 1954.

Zimmermann, A.: Flow resistance in steep streams: an experimental study. Water Resour. Res. 46. http://dx.doi.org/10.1029/2009WR007913, 2010.